

Structure of mammalian ornithine decarboxylase at 1.6 Å resolution: stereochemical implications of PLP-dependent amino acid decarboxylases

Andrew D Kern¹, Marcos A Oliveira¹, Philip Coffino² and Marvin L Hackert^{1*}

Background: Pyridoxal-5'-phosphate (PLP) dependent enzymes catalyze a broad range of reactions, resulting in bond cleavage at C α , C β , or C γ carbons of D and L amino acid substrates. Ornithine decarboxylase (ODC) is a PLP-dependent enzyme that controls a critical step in the biosynthesis of polyamines, small organic polycations whose controlled levels are essential for proper growth. ODC inhibition has applications for the treatment of certain cancers and parasitic ailments such as African sleeping sickness.

Results: The structure of truncated mouse ODC (mODC') was determined by multiple isomorphous replacement methods and refined to 1.6 Å resolution. This is the first structure of a Group IV decarboxylase. The monomer contains two domains: an α/β barrel that binds the cofactor, and a second domain consisting mostly of β structure. Only the dimer is catalytically active, as the active sites are constructed of residues from both monomers. The interactions stabilizing the dimer shed light on its regulation by antizyme. The overall structure and the environment of the cofactor are compared with those of alanine racemase.

Conclusions: The analysis of the mODC' structure and its comparison with alanine racemase, together with modeling studies of the external aldimine intermediate, provide insight into the stereochemical characteristics of PLP-dependent decarboxylation. The structure comparison reveals stereochemical differences with other PLP-dependent enzymes and the bacterial ODC. These characteristics may be exploited in the design of new inhibitors specific for eukaryotic and bacterial ODCs, and provide the basis for a detailed understanding of the mechanism by which these enzymes regulate reaction specificity.

Introduction

Pyridoxal-5'-phosphate (PLP) and pyridoxamine 5'-phosphate (PMP) are enzyme cofactors utilized extensively in amino acid metabolism [1]. The structure and evolution of vitamin B₆ dependent enzymes has recently been reviewed by Jansonius [2]. The B₆-dependent family of enzymes is described by four fold types represented by aspartate amino transferase [3] (fold-type I), tryptophan synthase β subunit [4] (fold-type II), alanine racemase [5] (fold-type III), and D-amino acid aminotransferase [6] (fold-type IV). These holoenzymes all contain an internal aldimine where the PLP is bound to an active-site lysine via a Schiff-base linkage. The amino acid substrate reacts with the cofactor via a transaldimination reaction to form an external aldimine. Any one of three remaining bonds around the C α carbon may be cleaved, enabling a broad range of reactions including transamination, racemization, retro-aldo cleavage, deamination, decarboxylation and replacement reactions [1]. This versatility of the PLP cofactor is demonstrated by its incorporation into at least

four distinct protein folds of widely varying polypeptide lengths, oligomeric forms, and with variable stabilities [2–14]. According to the Dunathan hypothesis [15], the sigma bond to be cleaved is oriented perpendicular to the plane of the pyridine ring in order to maximize overlap with the π system of conjugated double bonds, thereby stabilizing the negative charge generated upon bond cleavage. PLP-dependent enzymes achieve reaction specificity by positioning specific 'subsites' that interact with each of the groups surrounding the C α carbon of the substrate in a geometry that favors a particular bond cleavage. In decarboxylases, once the Michaelis–Menton complex is formed, transaldimination leads to the orientation of the α carboxylate perpendicular to the pyridine ring, followed by the release of CO₂ and the formation of a quinonoid intermediate [2]. The protonation of the quinonoid intermediate at the C α carbon may lead to retention or inversion of configuration. Retention of configuration is achieved when the proton donor lies on the same side of the pyridine ring as the leaving carboxylate

Addresses: ¹Department of Chemistry and Biochemistry, University of Texas at Austin, Austin, TX 78712, USA and ²Department of Microbiology and Immunology, School of Medicine, University of California at San Francisco, San Francisco, CA 94143, USA.

*Corresponding author.
E-mail: m.hackert@mail.utexas.edu

Key words: chemotherapy target, Group IV decarboxylase, polyamines, pyridoxal-5'-phosphate, obligate homodimer, stereochemistry

Received: 23 December 1998

Revisions requested: 8 February 1999

Revisions received: 25 February 1999

Accepted: 1 March 1999

Published: 3 May 1999

Structure May 1999, 7:567–581

<http://biomednet.com/elecref/0969212600700567>

© Elsevier Science Ltd ISSN 0969-2126

group. Inversion of configuration occurs by positioning the proton donor on the cofactor face opposite that of the leaving group.

Eukaryotic ornithine decarboxylase (ODC, EC 4.1.1.17) is a PLP-dependent enzyme. As a homodimer it produces putrescine (1,4-diaminobutane) from ornithine. This is the first committed step in polyamine biosynthesis [16]. Polyamines are ubiquitous aliphatic amines required for normal cell growth [17], they can be induced in response to hormones [18,19], and they lead to apoptosis when overabundant [20]. Constitutive ODC activity has been observed in cancer cells [21], and its uncontrolled expression confers a cancer phenotype on some cells [22]. Consequently, ODC inhibitors may be useful therapeutic agents in the treatment of certain cancers [23] and parasitic diseases [24]. Difluoromethylornithine (DFMO) is one ODC inhibitor undergoing clinical trials [25,26]. Knowledge of the different ODC folds may aid in the design of novel, ailment-specific ODC inhibitors.

Sequence comparisons of nine PLP-dependent decarboxylases arrange them into four sequence groups (Groups I–IV) [27]. However, structural comparisons reveal only two distinct PLP-binding folds for decarboxylases [28]. Groups I, II, and III share the PLP-binding motif (fold-type I) found in the bacterial ODC from *Lactobacillus 30a* (*L30a*ODC) [14]. Group IV decarboxylases, represented by mODC' (fold-type III), includes eukaryotic ODCs, diaminopimelate decarboxylase (DAPDC) and biosynthetic arginine decarboxylase. Secondary structure assignments based on comprehensive sequence comparisons correctly predicted that mODC' and alanine racemase (ALR) would contain an α/β -barrel domain [29], although the sheet assignments were different from those reported here.

The expression and activity of ODC in eukaryotes is controlled at many levels, including transcription, translation, post-translational modification [30–32], and a novel mechanism of selective protein degradation [33]. The latter involves a 25 kDa protein called antizyme (AZ) [34], which exploits the rapid monomer–dimer equilibrium exhibited by ODC [35], targeting ODC for degradation by the 26S proteasome [33,36]. AZ is itself regulated by AZ inhibitor [37], an enzymatically inactive protein that is homologous to ODC, but that binds more tightly to AZ [38].

In this report we describe the crystal structure of a truncated form of mouse ornithine decarboxylase (mODC'), which contains 424 of the 461 amino acids present in the native protein [39]. The omission of 37 C-terminal residues prevents degradation of the enzyme; the truncated protein retains catalytic activity [40]. The structure of mODC' is compared with that of the structurally homologous ALR [5], which also uses PLP as a cofactor.

We present a stereochemical model for mODC', correlating the structure with previous studies.

Results and discussion

ODC monomer is a two-domain structure

The secondary structure of the mODC' monomer is presented schematically (Figure 1a) together with a ribbon drawing of the monomer (Figure 1b) and an alignment of selected sequences of Group IV decarboxylases and ALR (Figure 1c). Each monomer is comprised of two domains, referred to in this paper simply as the barrel domain and the sheet domain. The crystal structure reveals that the two domains are linked by two neighboring loops, one preceding helix H2 and the other following H10. Residues 46–283 form an α/β barrel (the barrel domain), and the remaining residues form a mostly β structure (the sheet domain), which includes two sheets (S1 and S2).

The model of mODC' starts at residue 2 leading into β strand B1, followed by the antiparallel strand B2, then helix H1, which has one side buried by sheet S1. The barrel domain begins with a helix (H2) and ends with H10, unlike most triose phosphate isomerase (TIM) barrels which usually begin with a β strand [41]. S1 and S2 of the sheet domain twist onto one another, forming a central hydrophobic core. S1 is made up of seven strands (B1 \uparrow , B2 \downarrow , B18 \downarrow , B3 \downarrow , B12 \uparrow , B17 \downarrow , B14 \uparrow ; arrows represent the relative orientations of the strands) whereas S2 contains four (B12 \uparrow , B13 \downarrow , B15 \downarrow , B16 \uparrow). Two small helices (H11 and H12) cap one end of the sheet domain and are localized at the interdomain interface (Figures 1a and 1b). Strand B12 twists nearly 180°, connecting sheets S1 and S2. S2 has two central strands running parallel (B13 and B15), and the outer strands (B12 and B16) run antiparallel to the central strands. The outer strand B16 has a bulge of two residues.

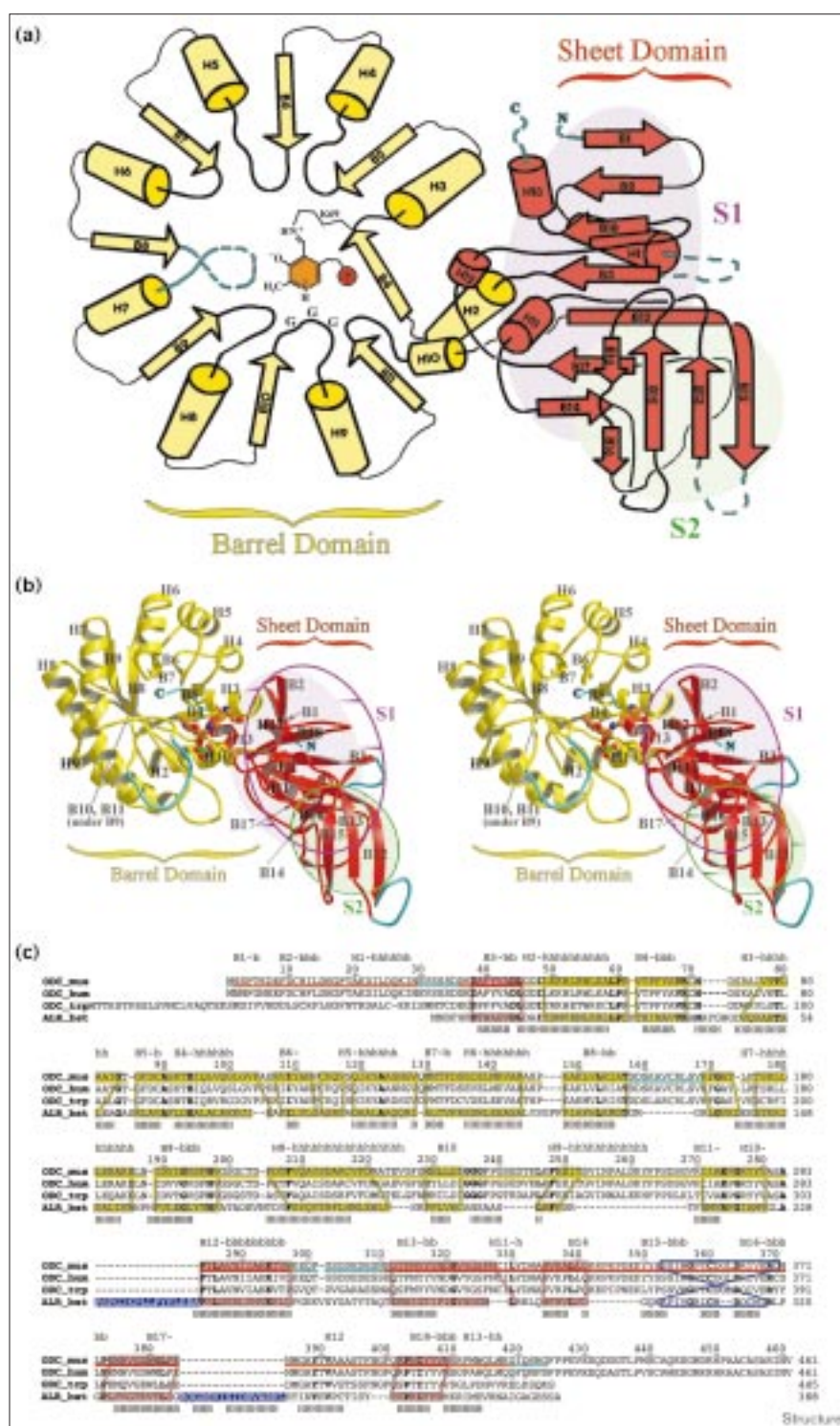
The model presented omits highly disordered residues (shown in cyan, Figure 1). In addition to one residue at the N terminus and six residues at the C terminus, there are three short disordered loops. One of these loops (158–168) connects H7 to B8 and corresponds to a protease-sensitive loop [42]. Sodium dodecyl sulfate polyacrylamide gel electrophoresis (SDS–PAGE) analysis of crystallized protein did not indicate proteolysis (data not shown). The remaining disordered loops connect H1 to B3 (30–35) and B12 to B13 (298–311). The latter loop is localized near the active-site cavity and includes the phosphorylation site S303 [32].

Dimer stability

Active ODC dimers are in rapid equilibrium with inactive monomers [43]. The structure of mODC' provides insight into mammalian ODC dimer instability, as only 655 Å² of solvent-accessible surface area per monomer is buried upon dimer formation. There is a clear separation

Figure 1

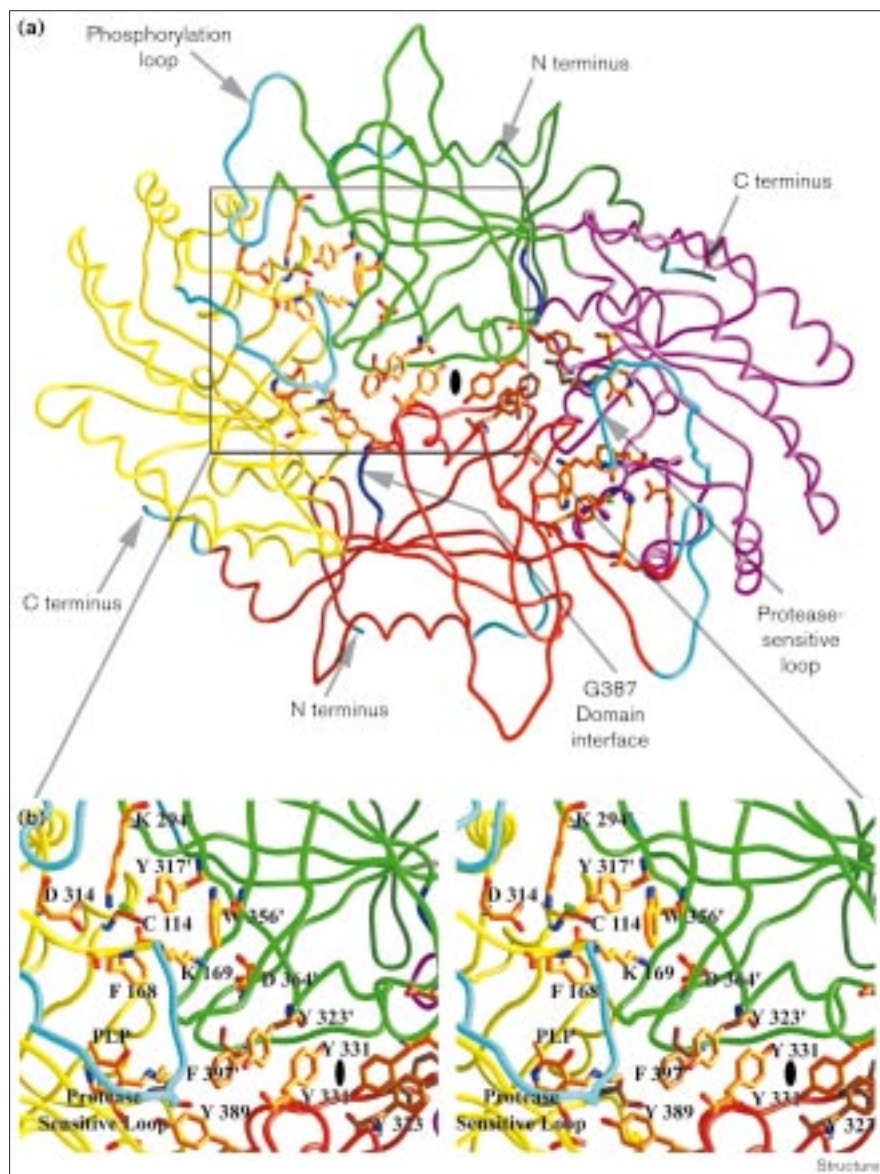
Structure of mODC'. The arrangement of the secondary structural elements of mODC' are depicted as a cartoon in (a) and shown as a ribbon drawing in (b) (generated using MOLSCRIPT [80] and Raster3D [81]). The barrel domain is shown in yellow and sheets S1 and S2 of the sheet domain are shown in red and highlighted with pink and green ovals, respectively. For mental reference, the disordered segments (colored in cyan) have the correct polypeptide lengths, but represent only potential conformations. Residues 425–461, which are part of mODC but not mODC', are omitted entirely. The sequence alignment of mODC' (ODC_mus), human ODC (ODC_hum), Trypanosomal ODC (ODC_trp) and alanine racemase (ALR_bst) is given in (c). The yellow, red, and cyan underscores follow the same scheme used in (a) and (b). The red and yellow boxes given in (c) indicate the structurally homologous regions, based on the structural superposition of mODC' and ALR. The blue boxes, shown in the alignment (c), indicate two insertions in ALR relative to ODC. The blue cross drawn between residues 353 and 370 of mODC and 303 and 316 of ALR indicate an area where mODC' and ALR show a topological inversion. The secondary structural elements of mODC' are given above its sequence following the nomenclature shown in (a). The secondary structural elements of ALR, according to [5], are given below the sequence of ALR in (c). Conserved residues are highlighted in bold.



between monomers within the homodimer (Figure 2). In contrast, *L30a*ODC dimers are very stable, involve intertwining of folding domains, and bury 6450 Å² upon dimer formation [14]. The mODC' dimer is easily disrupted by

any mutation to G387 [44]. G387 is located between the barrel and sheet domains (Figure 2), but is far removed from the dimer interface, suggesting that mutations at G387 are indirectly disrupting dimer formation, possibly

Figure 2



The mODC' dimer. (a) A backbone worm diagram of the mODC' dimer viewed down the twofold axis. One of the monomers is colored using the same color assignments as in Figure 1, whereas the second monomer has its barrel domain colored in magenta and the sheet domain in green. Key residues found at the dimer interface are drawn in (a) and labeled in the stereo enlargement (b). The sheet domains near the molecular twofold axis interact via two stacks of aromatic residues, and salt bridges are found at the edges of the dimer. G387, sandwiched between the barrel and sheet domains of a monomer, is shown colored in blue. Disordered polypeptide segments are colored in cyan. Note the relative locations of the cofactors at the C-terminal ends of the α/β -barrel domain (yellow and magenta), which open towards the twofold axis. This figure was produced using GRASP [82]. The twofold axis is indicated by a black disc.

by causing an alteration in angle between the barrel and sheet domains. An example of direct disruption through the introduction of a bulky residue has been demonstrated by G121Y in *L30 α* ODC (R Gopal, MAO, L Zhang, D Carroll and MLH, personal communication).

The symmetrical homodimer of mODC' is formed by a head-to-tail interaction between the barrel of one monomer and the sheet domain of the second (Figure 2). This model was proposed on the basis of site-directed mutagenesis of active-site residues [45] and the formation of functional cross-species heterodimers [46]. Two salt bridges (K169–D364' and D134–K294'; primed residues belong to the other monomer in the dimer) and

a stack of aromatic residues (F397'/Y323'/Y331 and Y331'/Y323'/F397) near the twofold axis form the primary interactions that stabilize the dimer (Figure 2). mODC is an obligate homodimer, and yet the size and shape of the interface and the small number of interactions stabilizing the dimer are very characteristic of nonobligatory complexes [47]. This characteristic is consistent with the observed rapid equilibrium [43] between mammalian ODC monomers and dimers, which appears to be needed for ODC regulation by AZ. AZ binds to ODC monomers and targets them for degradation by the 26S proteasome [33,36], but ODC dimerization apparently precludes antizyme binding [35]. The rapid equilibrium ensures a population of monomers, to which antizyme binds, and

LeChatelier's principle dictates that a depletion of the monomer population will ultimately result in the elimination of active dimers. It has been shown that residues 117–140 (H5–H6) are necessary for AZ binding [48]. Although the electrostatic surface of mODC' is mostly acidic, a basic patch is found at the N-terminal end of the barrel involving K121, K141 and R144 on helices H5 and H6 (Figures 1 and 3). This patch is not well exposed in the dimer, which could explain the preferential binding of antizyme to ODC monomers. Perhaps electrostatics will be found to play an important role in the relative binding affinities of AZ–mODC versus AZ–AZ-inhibitor, but a detailed analysis is beyond the scope of this paper.

Activity has been observed while expressing a circularly permuted mODC [49], and while co-expressing two fragments of *Trypanosoma brucei* ODC [42]. These experiments suggested that the location of the domain interface occurs around residue 305. The structure of mODC' reveals that this is not the case and that residue 305 is found on a disordered loop linking B12 to B13, within the sheet domain. Active, circularly permuted protein is made possible because of the flexibility and close spatial position of the C and N termini in the native structure. This enables the tethering of the N and C termini in the inverted protein while new termini are created at a disordered loop (298–311) of mODC'. The fact that the second experiment worked is fascinating. Cutting mODC' at residue 305 would produce a large and a small fragment. The large fragment would contain the entire barrel domain, linked with B12 and the majority of S1 (Figure 1), and the smaller fragment would contain the core portion of S2 linked with H12, B16, and H13. This S2 fragment contains all the active-site residues from the sheet domain, as well as most of the sheet domain's dimer contacts (Figure 2). The experiment strongly suggests that this S2 fragment can retain enough of its native conformation so that it is still able to interact with the barrel domain fragment to form a complete active site.

Comparison of fold with alanine racemase

A superposition of the α/β barrels of mODC' and ALR is shown in Figure 4a. This superposition gives a root mean square deviation (rmsd) of 2.5 Å for the C α carbons of 155 spatially equivalent residues (shown in yellow boxes, Figure 1c) from each barrel. These residues account for 65% and 70% of the residues found in the barrels of mODC' and ALR, respectively. The equivalent residues include the common core β structure and portions of the helices shared by mODC' and ALR. The dominant difference between the two barrels is found in the seventh helix of the barrel (H9 in mODC', Figure 4a). In mODC' H9 is a four-turn helix, far removed from the active site, preceded by a long loop containing a sequence fingerprint GGG (single-letter amino acid code), which is involved in the coordination of the PLP phosphate (Figure 4a). In ALR this helix is only two turns in length; it is located near the active site, is preceded and followed by short loops, and coordinates the PLP phosphate through S204 at its N-terminal end.

The superposition of the sheet domains (Figure 4b) gives an rmsd of 2.0 Å for the C α carbons of 64 residues from each sheet (shown in red boxes, Figure 1c). This accounts for 35% and 40% of the sheet domain residues of mODC' and ALR, respectively. The relative ($\sim 30^\circ$) rotation of the barrels becomes evident upon superposition of the sheet domains. The difference in the interdomain angle is caused by two insertions in ALR with respect to mODC' (shown in blue boxes, Figure 1c). The first is an interdomain insertion (229–244) between the eighth helix of the barrel and the ALR equivalent of mODC' B12 (Figures 1c and 4a). The second insertion within the sheet domain (334–349) gives rise to a β -hairpin loop and helix, which connect S2 and the very end of S1 in ALR (Figure 4b). The global superposition of all spatially equivalent residues between ALR and mODC' (155 from the barrel and 64 from the sheet domain of each enzyme) increases the rmsd to 4.3 Å.

Figure 3

Qualitative electrostatic surface potential of the mODC' monomer. The view in (a) shows the dimer oriented as in Figure 2, with the accessible surface area of the yellow–red monomer (disordered cyan regions are not included in the surface rendering). The view of the dimer in (b) is perpendicular to that shown in (a). A large electropositive patch located on the 'bottom' edge of the barrel includes residues 117–140, which have been implicated in antizyme interaction. The color coding is the same as in Figure 2. This figure was produced using GRASP [82].

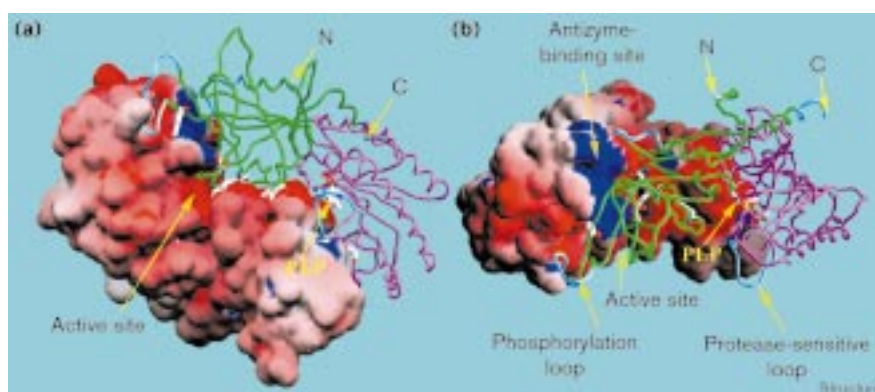
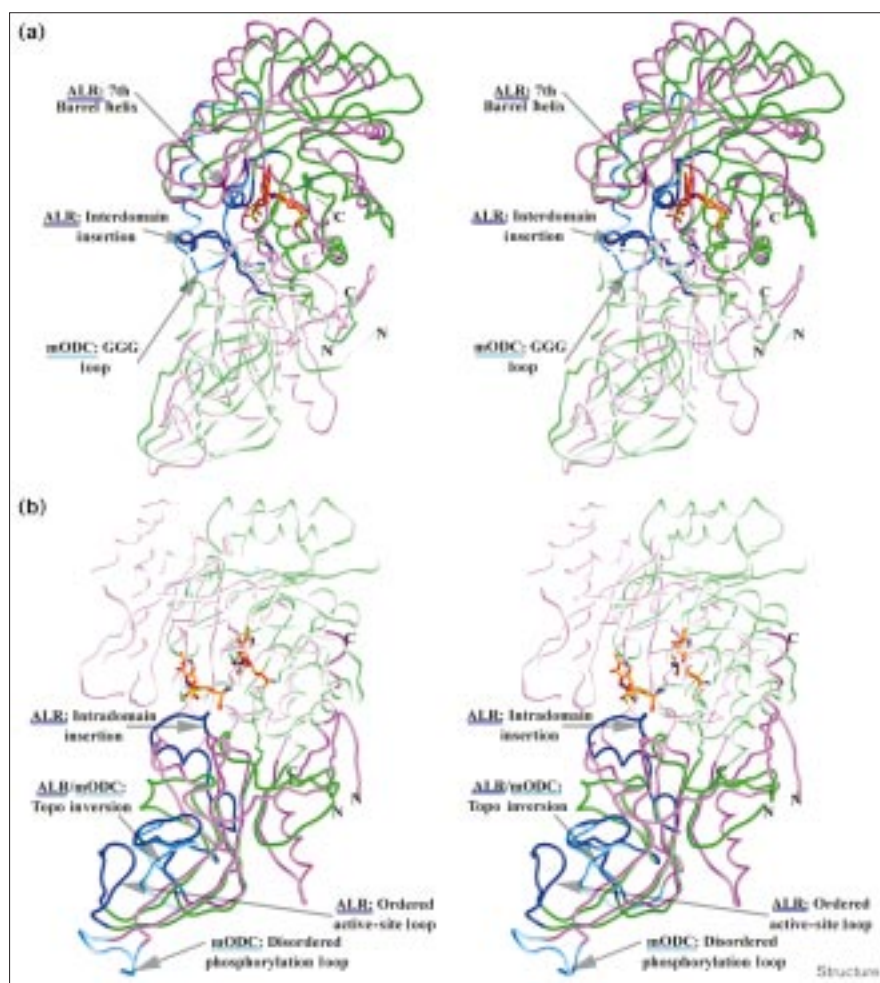


Figure 4



Structural comparison of mODC' and ALR (PDB accession code 1SFT). Comparison of mODC' (purple) and ALR (green) based on the superposition of the α/β barrels is illustrated in (a), with their respective sheet domains shown in faded colors. The comparison of the two structures based on the superposition of the sheet domains is shown in (b), using dimmed colors for the barrel domains. Notice in (b) how the superposition of the sheet domains enhances the difference in the angle between the barrel and sheet domains of the two structures ($\sim 30^\circ$). The cofactor is shown as a stick model in both (a) and (b). The unique portions of ALR are shown in blue whereas the corresponding regions in mODC' are shown in cyan. This figure was produced using GRASP [82].

The amount of surface area buried upon dimer formation is significantly different in mODC' and ALR, most probably a result of the interdomain-angle difference mentioned above. In mODC', 655 \AA^2 (13% of solvent-accessible surface area) per monomer are buried upon dimer formation, whereas in ALR 948 \AA^2 are buried (19% of solvent-accessible area) per monomer. The relatively smaller amount of buried surface area in mODC' is consistent with the observation of easily dissociable mODC dimers, which appear to be necessary for the regulation of mODC by AZ as described earlier.

Two other differences between mODC' and ALR are worth mentioning. The first is an interesting topological inversion (indicated by the crossed, blue lines in Figure 1c). This strand is found to contain active-site residues in each enzyme (C360', D361' in mODC'; C311', D313' in ALR) and occupies roughly the same space, and yet the directionality of the chain is reversed between the enzymes. The second difference pertains to a mobile loop that is disordered in the mODC' structure, but ordered in ALR. In

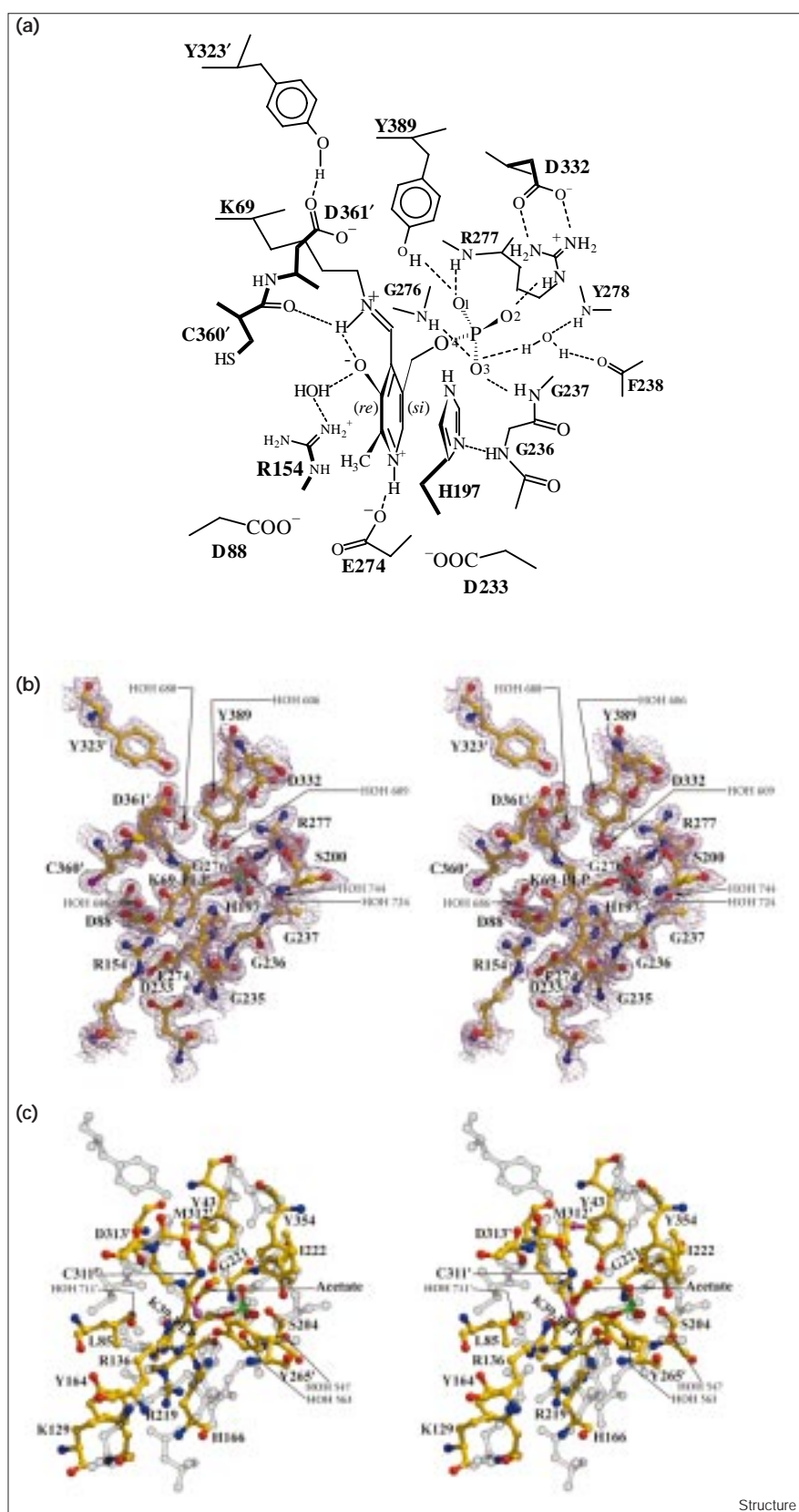
mODC' the disordered loop is found between strands B12 and B13, and it contains a potential phosphorylation site, S303 [32]. In ALR the loop contributes an important active site residue, Y265' [5].

Active site of mODC'

The PLP cofactor is bound via a Schiff base on the C-terminal end of the α/β barrel in a manner similar to that observed for other cofactors utilizing this fold. The active site is localized in a shallow cavity at the subunit interface (Figures 2 and 3). It is formed primarily from residues donated by loops from the C-terminal end of the α/β -barrel domain, one loop from the sheet domain (connecting B14 and B15 of S2) and two additional loops (357'–364', 398'–403') from the sheet domain of the second monomer. One of the salt bridges (K169–D364') that stabilizes the dimer fixes the loop containing residues C360', D361' and D364' from the neighboring monomer to complete the active site (Figure 2). This is in agreement with the observed loss of activity when K169 is mutated [50].

Figure 5

Active site of mODC' and comparison with ALR. (a) Schematic drawing of the mODC' active site illustrating the hydrogen-bond interactions. Residues shown in bold face are nearer the viewer. (b) Stereo figure of the active site of mODC' with electron density superimposed with its model. K69 of mODC' is in Schiff-base linkage to the cofactor, E274 pairs with the pyridine ring nitrogen N1, and H197 stacks on the *si* face of the cofactor ring. Note the angle between K69 and the pyridine ring of the cofactor exposing the *si* face. The map is a $2F_o - F_c$ map at 1.6 Å resolution contoured at 1.2σ . (c) A view of the ALR and mODC' active sites resulting from the superposition of their cofactor rings. The mODC' active site is depicted in light gray. The figures were generated using BOBSCRIPT [83], MOLSCRIPT [80] and Raster3D [81].



Structure

Table 1

Comparison of the protein interactions with pyridoxal-5'-phosphate linked to ALR and mODC*.

Cofactor atoms	mODC' (distances in Å)		ALR (distances in Å)	
PLP/LYS NZ	HOH 688	O	3.2	no equivalent
	C360'	O	3.0	no equivalent
PLP N1	E274	OE1	2.7	R219 NE 2.7
PLP O3	HOH 686	O	2.5	HOH 711' O 2.8
				R136 NH2 3.1
	C360'	O	3.1	no equivalent
PLP O1P				acetate OXT 3.2
	Y389	OH	2.5	Y43 OH 2.7
	R277	N	2.8	I222 N 2.8
PLP O2P	R277	NE	2.9	Y354 OH 2.9
	HOH 724	O	2.5	HOH 563 O 2.7
				HOH 547 O 3.0
PLP O3P	HOH 744	O	2.7	S204 OG 2.7
	G237	N	2.9	S204 N 3.0
	G276	N	3.0	G221 N 3.2

*See Figure 7.

The position and orientation of the cofactor in the active site is governed primarily by protein interactions with the 5'-phosphate and the pyridine nitrogen, N1 (Figure 5a,b). The phosphate binds in a pocket formed by two loops (235–241, 274–276) and the N terminus of H10. One of these loops contains the GGG sequence (residues 235–237), which is conserved in all Group IV PLP-dependent decarboxylases, and the other loop connects B11 to H10. Both loops contribute hydrogen bonds involving mainchain nitrogens (G237, G276, R277). R277, at the N terminus of H10, contributes a hydrogen bond to the phosphate via its Nε, while the Nε nitrogens are held in place by a salt bridge to D332. This salt bridge restrains R277 while interconnecting the barrel and sheet domains. Studies of an R277A mutant, at the optimal pH (8.0), shows a ~100-fold decrease in PLP binding as well as a 50% drop in k_{cat} and a ~sevenfold decrease in K_M [51]. The 5' phosphate is further fixed by a hydrogen bond to Y389 (Figure 5a,b). Interestingly, a similar tyrosine is found with the same geometry in aspartate aminotransferase [3], the fold of which more closely resembles that of the bacterial *L30α*ODC [14]. A tightly bound water molecule (HOH 744), interacting with a carbonyl (F238) and a mainchain nitrogen (Y278), is found buried beneath the phosphate, hydrogen-bonded to O3P. The primary interaction of N1–PLP is with E274 [52]. It is part of a cluster of acidic residues (D88, E274, D233) that, with three bound water molecules (Figure 5b), form a network of hydrogen bonds that probably influences the electron-withdrawing properties of the cofactor.

The extensive number of interactions between mODC' and the 5' phosphate is consistent with the PLP binding constant observed for trypanosomal ODC ($K_D < 0.05 \mu\text{M}$ at optimal pH of 8.0, [51]). Characterizations of native

mODC' and the R277A mutant using ^{31}P nuclear magnetic resonance (NMR) spectroscopy suggest that the phosphate is bound in a strained conformation relative to other PLP-dependent enzymes. The active site of mODC' is highly hydrophilic and shows a number of ordered waters. This is in contrast to other PLP enzymes (i.e. ALR, L-Aspartate amino transferase (L-AspAT), *L30α*ODC, and tryptophan synthase), where one face of the cofactor is usually buried against a hydrophobic surface [5,3,4,14]. Thus, in order to have a better control over catalytic intermediates that are linked to PLP it is important to fix the phosphate tightly.

The environment of the pyridine ring and its other substituents (Figure 5a,b) also affects enzyme activity [53]. The methyl group, commonly found in a hydrophobic environment, is observed in a hydrophilic environment generated by R154, E274, and bound solvent molecules. The hydroxyl group is within hydrogen-bonding distance (3.1 Å) of the backbone carbonyl of C360', which is also 3.0 Å from the aldimine nitrogen atom of the pyridine ring (Figure 5), suggesting that the carbonyl of C360' could be involved in stabilization of the quinonoid intermediate. This scenario is in sharp contrast to *L30α*ODC, where the aldimine nitrogen is hydrogen-bonded to the hydroxyl group of the pyridine ring and is found in the plane of the pyridine ring [14].

Comparison with the ALR active site

Comparison of the structures of mODC' with ALR reveals that residues governing cofactor binding are more conserved than those that determine the catalytic potential and the stereospecificity of the reaction. The phosphate and N1 nitrogen act as pivot points, anchoring the cofactor as it swings between internal and external aldimine forms during a catalytic cycle. Superposition optimized on just the two cofactor rings results in an increase of the rms fit of the selected barrel residues from 2.5 Å to 7.5 Å, indicating that the two cofactors do not sit identically within their respective barrels. However, overlapping the two cofactors is an excellent way of viewing the cofactor environments in the two enzymes (Figure 5c).

The comparison of the phosphate environment shows significant similarity with Y389 of mODC' closely overlapping Y43 of ALR. Both tyrosines form hydrogen bonds to O1P of the cofactor. A comparison of the cofactor hydrogen bonds in the two active sites is shown in Table 1. It can be seen that both enzymes immobilize the cofactor phosphate using backbone nitrogens. The backbone nitrogens of G276, R277, and G237 in mODC' are equivalent to G221, I222, and S204 in ALR. The sidechain of S204 in ALR also provides a hydrogen bond to O3P, which is replaced by a water molecule in mODC'. The sidechain interaction of R277 with the phosphate in mODC' is replaced by Y354 in ALR. The

arginine in mODC' would be expected to provide much tighter binding.

There is a striking difference in the environments around N1 in both structures. In most PLP-dependent enzymes, an acidic group (E274 in the case of mODC') is usually found to interact with the pyridine nitrogen (N1), whereas in ALR the group (R292, [5]) is basic. The basic environment around N1 in ALR has two potential effects, as suggested by Shaw *et al.* [5]. The first effect is a decrease in the pKa of the N1 nitrogen, keeping it less protonated, and diminishing its electron-withdrawing capabilities relative to mODC'. R292 will also affect the protonation state of the imine nitrogen, influencing the efficiency of the transaldimination step of ALR. In contrast, in mODC' the presence of three acidic groups (D88, D233, and E274) near the N1 nitrogen probably enhances activity by increasing the pKa of N1. This view is consistent with data suggesting that the pKa of N1 is 8.5 [51], and that the slowest step in the reaction of the *trypanosomal* ODC is product release [54].

In mODC', both faces of the pyridine ring (*re* and *si*, Figure 5a) are surrounded by hydrophilic residues, even the buried *re* side faces a small hydrophilic cavity; whereas in ALR the buried *re* face is in a tight, hydrophobic environment. The cofactor methyl group of mODC' is in a hydrophilic environment, near R154, whereas in ALR the methyl is near the hydrophobic regions of Y164 and L85. Interactions surrounding the pyridine hydroxyl affect the pKa of the imine nitrogen, regulating the efficiency of transaldimination. The network of interactions involving the pyridine hydroxyl of mODC' probably favors the attack by the incoming amino group of the substrate by keeping the imine nitrogen protonated [54]. In mODC' the pyridine hydroxyl group is within hydrogen-bonding distance of a water (HOH 686, Figure 5b), whereas in ALR an equivalent water (HOH 711') bridges the hydroxyl and an arginine (R136, Figure 5c). The main-chain carbonyl of C360' of mODC' is within 3.0 Å of the imine nitrogen, but also within 3.1 Å of the PLP O3P, and it is potentially hydrogen-bonded to the proton shared by those groups.

mODC' and ALR have distinct ways of immobilizing a histidine sidechain next to the cofactor (H197 in mODC' and H166 in ALR). The angle between the plane of the imidazole ring and the pyridine ring is significantly different in the two enzymes. The imidazole ring of H197 in mODC' shares a hydrogen bond via its Nε2 nitrogen with the backbone nitrogen of G236, but its Nδ1 nitrogen is free, allowing the plane of the imidazole ring to be within 10° of stacking parallel against the pyridine ring. In contrast, H166 of ALR requires a rotation of 35° to make these rings parallel. In ALR the two rings are held even more rigidly with respect to each other by having the

cofactor pyridine nitrogen and the sidechain of H166 both interact with the sidechain of R219. In addition, the other side of the H166 imidazole is hydrogen-bonded to Y265', a residue localized in a sheet domain of a neighboring monomer in the dimer. This dual interaction essentially fixes the H166 of ALR in place, controlling the angle of the imidazole ring with respect to the pyridine ring; this suggests a potential mechanism for tuning the pKa of Y265', which is thought to be a catalytic base in the reaction of ALR [5,55].

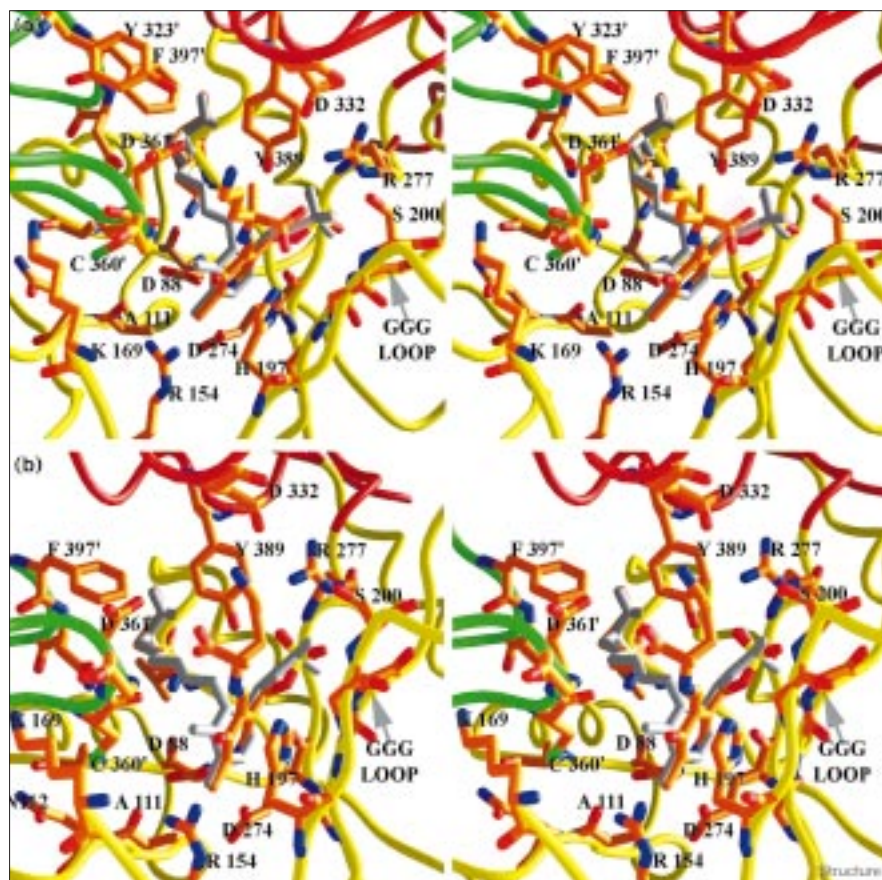
In both mODC' and ALR, the active site is composed in part by a substrate-specificity loop from the sheet domain of the neighboring monomer. This loop includes a cysteine and an aspartate (C360' and D361' in mODC'; C311' and D313' in ALR). The topological inversion of this loop in mODC' (Figure 4b) is probably related to the differences in substrate specificity of the two enzymes (Figure 5).

Stereochemical properties

When studying the mechanisms of related enzymes it is important to compare the chiral fidelity of their reactions. The stereochemistry of PLP-dependent reactions involves coenzyme face selectivity with respect to three characteristics: the mode of cofactor binding, burying one of its two faces (*re* or *si*); the orientation of the labile sigma bond perpendicular to the pyridine ring, positioning the cleaved substituent on either (*re* or *si*) face; and the position of general acid/base groups on either or both faces of the cofactor. The stereochemical characteristics of the PLP-dependent transaminase L-AspAT have been extensively studied [56–63]. Transaminases use PLP or PMP for the interconversion of keto acids and amino acids catalyzing a stereospecific 1,3 prototropic shift whereby a proton is abstracted from the Cα carbon and donated to the C4' atom of the cofactor on the buried *si* face [56]. In ODC, true chirality around Cα is lost when the substrate is converted to putrescine; thus, any meaningful experiments in this regard would require the use of deuterium or tritium to determine if the Cα has undergone racemization, retention or inversion of its configuration. Unfortunately, no such experiments have been reported for mODC.

In order to gain insight into the stereochemistry of mODC', we have modeled the external aldimine form of L-α-methylornithine in the active site of mODC'. The use of the L-α-methyl derivative of ornithine aids the visualization of stereochemistry and has relevance in that the monofluoro and difluoromethylornithines are potent inhibitors of the enzyme. L-α-methylornithine is easily accommodated because of the openness of that region in the active site. There are only two ways of orienting the carboxylate group of the substrate in the external aldimine complex such that it is placed perpendicular to the pyridine ring, satisfying the Dunathan hypothesis [15] for

Figure 6



Models of two potential orientations of the external aldimine form of L- α -methylornithine in the active site of mODC'. (a) Model of the external aldimine shown with its carboxylate oriented towards the exposed, *si* face of the cofactor where H197 is localized. (b) Model of the external aldimine shown with its carboxylate pointed towards the buried *re* face of PLP, on the same side as K69. Notice how the orientation of the external aldimine shown in (a) positions the N ϵ terminal amino group of L- α -methylornithine in a more favorable position, relative to (b), closer to the substrate-determinant site, D361'. The molecule depicted in gray is the cofactor orientation as observed in the native structure. The program SYBYL (Tripos) was used to build and energy minimize both possibilities into the active site of mODC'.

cleavage of the C α -CO₂ bond (Figure 6). In accordance with the observation of the external aldimine form in L-AspAT, in both models the cofactor was tilted 30° using the phosphate and the N1 atom of pyridine as a hinge [58].

As D361' is the primary substrate-binding determinant [52], interactions with this residue can be used as a criterion in evaluating the preferred orientation of the two external aldimine complexes. The models (Figure 6) suggest that the most favorable orientation of the labile C α -CO₂ bond orients the carboxylate group on the exposed *si* face of the cofactor (opposite K69 and C360'). This positions the terminal N ϵ of L- α -methylornithine only ~3.0 Å from D361'. In contrast, orienting the carboxylate group on the buried *re* face of the cofactor (nearer K69 and C360') positions N ϵ of the ornithine sidechain away from D361' and close to the salt bridge D332-R277. Site-directed mutagenesis of D361A principally shows a K_M effect [52], whereas mutation of K69A results in a 561-fold reduction of k_{cat} [64]. A mutation similar to K69 in L-AspAT (K258A) provides evidence of its role as an acid/base catalyst in the transaminase reaction [60]. Together, these data and our modeling studies suggest that, like DAPDC [65], decarboxylation in

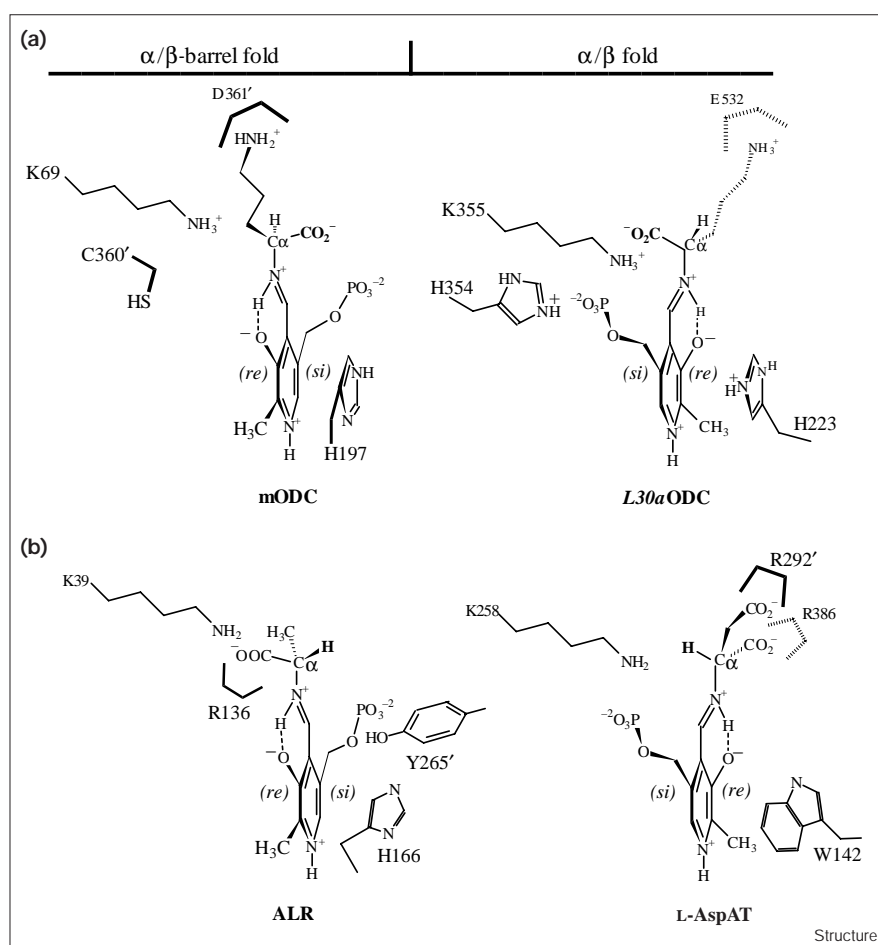
mODC' should occur with inversion of configuration about C α .

One notable difference between the active-sites of mODC' and ALR lies in the structure of an active-site loop from the neighboring sheet domain. In ALR this loop (259-273) is ordered and contains a proposed base (Y265'), which interacts directly with PLP. The equivalent loop in mODC' (298-311) is disordered, but biochemical data show that this loop contains a phosphorylation site (S303). Although a conformational change of this loop upon substrate binding cannot be ruled out, its acidic composition suggests that a 'closed' state would lead to a more negatively charged environment on the *si* face of the cofactor. This should enhance removal of CO₂ oriented in the *si* face (Figure 6) of the cofactor and stabilize the quinonoid intermediate. Phosphorylation of this loop would be expected to enhance this effect. Indeed, mODC demonstrates enhanced activity when phosphorylated at multiple sites *in vivo*, but, surprisingly, phosphorylation of S303 alone has no effect on catalytic activity [31,32].

Our data are consistent with the view that PLP-dependent enzymes having fold-type I, II, or IV [2] perform bond

Figure 7

Schematic diagrams illustrating the external aldimine forms of the cofactors in PLP-dependent decarboxylases, transaminases, and racemases. This cartoon shows the relative positions of potential proton donors with respect to the cofactor faces. mODC and ALR have their *si* face exposed to solvent, whereas *L30a*ODC and L-AspAT have the *re* face exposed. The accession codes are: ALR (1SFT), *L30a*ODC (1ORD) and L-AspAT (9AAT).



cleavage and proton donation/abstraction on the buried face of the cofactor. Fold-types I and II bury the *si* face of PLP whereas fold-type IV buries the *re* face. PLP-dependent decarboxylases, classified into four sequence groups on the basis of sequence analysis [27], fall into two structural PLP-dependent enzyme fold types [28]. Groups I, II and III belong to fold-type I (~L-AspAT) and sequence group IV has fold-type III (~ALR). Fold-type I decarboxylases bind PLP with the *si* face buried along with the catalytic lysine residue and possess substrate determinants that position the carboxylate in the buried face of the cofactor. Like its transaminase relative L-AspAT, *E. coli* ODC catalyses a stereospecific reaction on the buried *si* face of the cofactor [66]. Thus, decarboxylases of fold-type I (*L30a*ODC) should function via retention of configuration about C α . In contrast, fold III enzymes (mODC, ALR and DAPDC) have an α/β -barrel fold, bind PLP with its *si* face exposed opposite the Schiff-base lysine residue, and may have evolved to function nonstereospecifically. This view is supported by data obtained with racemases (ALR), which can perform nonstereospecific transamination as a

side reaction [67], and DAPDC, where inversion of configuration about C α was observed [65]. Although suggested by this analysis, it remains to be confirmed whether or not all fold-type III decarboxylases work with inversion of configuration about C α .

A striking example of convergent evolution is noted in the structures of amino acid transaminases. D-amino acid transaminase binds PLP with the *si* face exposed to solvent [6] whereas in L-AspAT the *re* face is exposed [3]. By maintaining the relative orientations of the proton donor and leaving groups, the site of the 1,3 prototropic shift is kept buried, requiring a rearrangement of the substrate-specificity site because of the differences in the chirality of the substrate. As suggested by Grishin *et al.* [29], there may still be other yet unknown PLP-binding folds, which may increase the chemical diversity described here.

Potential proton donors

Although the identity of the proton donor in the reaction of mODC is not yet known, there are three potential

Table 2

X-ray diffraction data.				
Data set	Resolution (Å), redundancy	Completeness (%) (All/outer shell)	R _{merge} (%) [*] (All/outer shell)	MIR statistics [†] (R _c /PP)
Native	1.6 / 5.0	91.3 / 75.4	8.1 / 18.8	
EMTS1 [†]	2.8 / 12.6	99.7 / 100.0	10.8 / 26.9	0.67 / 1.84
EMTS2 [†]	2.7 / 9.6	91.5 / 92.9	5.3 / 6.4	0.59 / 2.84
K ₂ PtCl ₆	2.8 / 4.5	92.0 / 88.7	4.7 / 8.1	0.92 / 0.71
K ₂ Pt(NO ₂) ₄	2.8 / 7.0	92.7 / 97.0	4.9 / 7.4	0.85 / 1.00

[†]EMTS = ethylmercurithiosalicylic acid. EMTS1 was collected in-house, RAXIS-4 detector (Molecular Structures Corporation), room temperature, $\lambda = 1.54$. All other data sets were collected at CHESS, -175°C , $\lambda = 0.918$. ^{*}R_{merge}(%) = $100 \times \sum_h (\sum_i |I_{hi} - \langle I_h \rangle| / \sum_i I_{hi})$. The values given are those reported by SCALEPACK. The R_{culis} (RC), and phasing power (PP) values given are those reported by MLPHARE.

donors: two on the *re* face of the cofactor (K69 and C360') and one on the *si* face (H197) (Figure 7a). Alanine mutations at positions K69 and C360 show a stronger k_{cat} effect for the K69A mutant than the C360A mutant [64]. This implies that the proton donor involved in the reprotonation of C α is probably K69, but C360' may serve that purpose in the K69A mutant. Although K69 and C360' appear to be far apart in the structure of mODC' (SH...NH > 5 Å) (Figure 5b), a rotation of the C360' sidechain about χ_1 would put the sulfhydryl of C360' within 3–4 Å of the K69 N ζ .

On the *si* face of the cofactor H197 is nearly stacked against the pyridine ring about 4.6 Å away from the pyridoxal phosphate but hydrogen-bonded to the amide nitrogen of G236. This hydrogen bond is very important in that it connects H197 to a chain of four backbone

hydrogen-bond interactions capped by R107. Thus, H197 is an unlikely proton donor because of the higher pK_a of the arginine guanidinium with respect to the histidine imidazole. This suggests that the primary purpose for the hydrogen bond with G236 is to anchor the imidazole ring of H197 in place, possibly stabilizing reaction intermediates. A similar histidine (H223) is observed in *L30a*ODC, where it too is found on the opposite side relative to the lysine forming a Schiff base with PLP (Figure 7b). Stereochemical studies of the bacterial ODC [66] show retention of configuration about C α , suggesting that H223 in *L30a*ODC is not the proton donor, but that it probably stabilizes PLP in its active site via base stacking of the aromatic rings.

In the bacterial *L30a*ODC, like in *L*-AspAT, the potential bases in the reaction are found on the buried *si* face of the cofactor (Figure 7b and 7d). As the proposed substrate specificity site of *L30a*ODC (E532) orients the carboxylate on the *si* face [12] where the potential bases are found (Figure 7b), retention of configuration is expected, and observed, in *E. coli* ODC [66]. In contrast to bacterial ODC's, mODC' has the *re* face buried along with the Schiff-base lysine K69 (Figure 7a).

Biological implications

Ornithine decarboxylase (ODC) is a key enzyme in polyamine biosynthesis; polyamines are small organic cations essential for life. ODC inhibitors may be useful therapeutic agents in the treatment of certain cancers and parasitic diseases. Difluoromethylornithine (DFMO) is one ODC inhibitor undergoing clinical trials. Models of host and parasite ODCs might aid in the design of novel, ailment-specific inhibitors.

Cells can quickly modulate ODC activity over a large dynamic range by altering the rate of ODC transcription and translation, but pre-eminently by modifying the half-life of the enzyme [68]. The present studies further our understanding of the catalytic function of the enzyme, confirming a series of expectations regarding the active

Table 3

Phasing and refinement statistics.

Overall FOM (2.7 Å) before solvent flattening [*]	0.82
Resolution (Å)	28.0–1.6
R _{factor} /R _{free} [†]	20.0/23.4
Space group	P2 ₁ 2 ₁ 2 (a = 118.8 b = 74.0 c = 45.6)
No. of non-H atoms in asymmetric unit [‡]	
protein	3045
water	421
Average B factors (Å ²)	
protein	21.3
water	34.0
Rms deviations [§]	
bond lengths (Å)	0.010
bond angles (°)	2.188
dihedral angles (°)	25.478
improper angles (°)	1.949
Ramachandran plot	98% core, 2% outliers

The ^{*}figure of merit (FOM) value is that reported by MLPHARE. [†]R_{free} was calculated with 4% Native (1995 reflections in the R_{free} set). The values given are those reported by REFMAC. No sigma cutoff was applied, to any of the data, for any of the statistics reported in this table. [‡]There is one monomer per asymmetric unit. Hydrogen atoms are not included in the number of atoms. [§]Rms (root mean square) deviations were produced using X-PLOR.

site that were based on studies of ODC mutants. In particular, as previously conjectured, each of the two active sites within the enzyme homodimer lies at the subunit interface and each contains essential elements from both monomers. The ODC homodimer equilibrium only modestly favors dimer formation. This result is consistent with our model, which shows that only a small fraction of monomer solvent-accessible surface area is buried upon dimer formation. The interaction with a second protein, antizyme (AZ), converts the ODC homodimer to an ODC-AZ heterodimer. This has two consequences: the enzyme is inactivated, because disruption of the homodimer disassembles the catalytic site; and ODC is degraded by the proteasome, the major neutral protease of the cell, because ODC, when associated with AZ, is efficiently recognized and degraded by the proteasome. The proteasome causes ODC to be destroyed and AZ to be recycled for further use. ODC is unusual among proteasome substrates. Almost all others require that post-translational modification by multiple copies of the protein ubiquitin take place before proteolysis. In contrast, ODC forms a tight but noncovalent 1:1 stoichiometric complex with AZ before degradation. The structure of the ODC-AZ complex and its features that specify proteasome recognition and processing remain to be determined.

Materials and methods

Crystallization

Native conditions described here are different from those that produced crystals previously analyzed at Stanford synchrotron radiation laboratory (SSRL) [39]. All solutions are at pH 6.5 and have 40 mM PIPES-KOH and 0.02% (w/v) Na₃. In addition, protein solution (PS) = 12 mgml⁻¹ mODC', 2.5 mM DTT, 1.0 mM EDTA; well solution (WS) = 26% (w/v) PEG 3350; equilibrating solution (ES) = 10% (w/v) PEG 3350; stabilizing solution (SS) = 30% (w/v) PEG 3350. Native crystals are grown as follows: 10 µl of silica hydrogel (Hampton Research) on a microbridge, sitting within a 3.25 ml well containing 1.0 ml ES, is gently covered with 10 µl WS. The well is sealed with tape and equilibrated at room temperature for one week. The microbridge is transferred to a well containing 1.0 ml WS. PS (20 µl) is added to the microbridge and the well is sealed with tape. The plate is left undisturbed in the dark at room temperature for two weeks. Crystals will often be 0.5 mm in length. The microbridge is then transferred to a well that contains 1.0 ml SS and the well sealed. If this last step is omitted, the crystals will begin to have tattered edges and degrade. Reproducibility varies with protein freshness and with each batch of protein that is prepared. Crystals were taken from microbridges and flash cooled to -175°C.

Structure determination and refinement

The ethylmercurithiosalicylic acid. (MTS1) derivative (Table 2) was collected both at Cornell high energy synchrotron source (CHESS) and in-house, using an RAXIS-4 detector (Molecular Structures Corporation), room temperature, $\lambda = 1.54 \text{ \AA}$. All other data sets were collected at CHESS F1 station using a Princeton charged-coupled device (CCD) detector [69], -175°C, $\lambda = 0.918 \text{ \AA}$. All metal derivatives were soaks of crystals from the same batch used to the collect native data set. The X-ray data were processed and merged using the programs DENZO and SCALEPACK [70]. The program MLPHARE [71] was used to obtain the original MIR phases. The wARP script [72] was used to obtain a highly interpretable map. Model building

was performed using the program O [73]. X-PLOR [74], version 3.851, was used for energy minimization, torsion dynamics while extending phases from 2.8 to 1.6 Å resolution and for picking waters. Final refinements at 1.6 Å resolution were performed using REFMAC [75] (Table 3). X-PLOR [74], PROCHECK [76] and WHAT_CHECK [77] were used for structural analysis. 6D_MOLEMAN [78] was used for structural analysis and file manipulation. Several CCP4 programs/utilities were also used [79].

Accession numbers

Coordinates have been deposited in the Brookhaven Protein Data Bank with accession code 7ODC.

Supplementary material

Additional material is available with the internet version of this paper.

Acknowledgements

This work was supported in part by grants to MLH from the National Institutes of Health (GM30105) and the Foundation for Research, and to PC by NIH grant GM45335. We thank Nick Grishin for help with the sequence alignment shown in Figure 1c. This work is based upon research conducted at the Cornell High Energy Synchrotron Source (CHESS), which is supported by the National Science Foundation under award DMR-9311772, using the Macromolecular Diffraction at CHESS (MacCHESS) facility, which is supported by award RR-01646 from the National Institutes of Health. This work is also based in part upon research conducted at the Stanford Synchrotron Radiation Laboratory (SSRL), which is funded by the Department of Energy, Office of Basic Energy Sciences. The Biotechnology Program is supported by the National Institutes of Health, National Center for Research Resources, Biomedical Technology Program and the Department of Energy, Office of Biological and Environmental Research. We acknowledge the staff at both CHESS and SSRL for assistance with data collection.

References

- Martell, A.E. (1982). Reaction pathways and mechanisms of pyridoxal catalysis. *Adv. Enzymol. Relat. Areas Mol. Biol.* **53**, 163-199.
- Jansonius, J.N. (1998). Structure, evolution and action of vitamin B6-dependent enzymes. *Curr. Opin. Struct. Biol.* **8**, 759-769.
- Ford, G.C., Eichele, G. & Jansonius, J.N. (1980). Three-dimensional structure of a pyridoxal-phosphate-dependent enzyme, mitochondrial aspartate aminotransferase. *Proc. Natl Acad. Sci. USA* **77**, 2559-2563.
- Hyde, C.C., Ahmed, S.A., Padlan, E.A., Miles, E.W. & Davies, D.R. (1988). Three-dimensional structure of the tryptophan synthase $\alpha_2\beta_2$ multienzyme complex from *Salmonella typhimurium*. *J. Biol. Chem.* **263**, 17857-17871.
- Shaw, J.P., Petsko, G.A. & Ringe, D. (1997). Determination of the structure of alanine racemase from *Bacillus stearothermophilus* at 1.9 Å resolution. *Biochemistry* **36**, 1329-1342.
- Sugio, S., Petsko, G.A., Manning, J.M., Soda, K. & Ringe, D. (1995). Crystal structure of a D-amino acid aminotransferase: How the protein controls stereoselectivity. *Biochemistry* **34**, 9661-9669.
- Gallagher, D.T., *et al.*, & Eisenstein, E. (1998). Structure and control of pyridoxal phosphate dependent allosteric threonine deaminase. *Structure* **6**, 465-475.
- Isupov, M.N., *et al.*, & Harutyunyan, E.H. (1998). Crystal structure of tryptophanase. *J. Mol. Biol.* **276**, 603-623.
- Shen, B.W., Hennig, M., Hohenester, E., Jansonius, J.N. & Schimer, T. (1998). Crystal structure of human recombinant ornithine aminotransferase. *J. Mol. Biol.* **277**, 81-102.
- Hennig, M., Grimm, B., Constestabile, R., John, R.A. & Jansonius, J.N. (1997). Crystal structure of glutamate-1-semialdehyde aminotransferase: an α_2 -dimeric vitamin B6-dependent enzyme with asymmetry in structure and active site reactivity. *Proc. Natl Acad. Sci. USA* **94**, 4866-4871.
- Clausen, T., Huber, R., Laber, B., Pohlenz, H.D. & Messerschmidt, A. (1996). Crystal structure of the pyridoxal-5'-phosphate dependent cystathionine β -lyase from *Escherichia coli* at 1.83 Å. *J. Mol. Biol.* **262**, 202-224.
- Toney, M.D., Hohenester, E., Cowan, S.W. & Jansonius, J.N. (1993). Diallylglycine decarboxylase structure: Bifunctional active site and alkali metal sites. *Science* **261**, 756-759.
- Antson, A.A., *et al.*, & Wilson, K.S. (1993). Three-dimensional structure of tyrosine phenol-lyase. *Biochemistry* **32**, 4195-4206.

14. Momany, C., Ernst, S., Ghosh, R., Chang, N. L. & Hackert, M. L. (1995). Crystallographic structure of a PLP-dependent ornithine decarboxylase from *Lactobacillus 30a* to 3.0 Å resolution. *J. Mol. Biol.* **252**, 643-655.
15. Dunathan H.C. (1966). Conformation and reaction specificity in pyridoxal phosphate enzymes. *Proc. Natl Acad. Sci. USA* **55**, 712-716.
16. Tabor, C.W. & Tabor, H. (1984). Polyamines. *Annu. Rev. Biochem.* **53**, 749-790.
17. Luk, G.D., Civin, C.I., Weissman, R.M. & Baylin, S.B. (1982). Ornithine decarboxylase: essential in proliferation but not differentiation of human promyelocytic leukemia cells. *Science* **216**, 75-77.
18. Cohen, S., O'Malley, B.W. & Stastny, M. (1970). Estrogenic induction of ornithine decarboxylase *in vivo* and *in vitro*. *Science* **170**, 336-338.
19. Russel, D. & Snyder, S.H. (1968). Amine synthesis in rapidly growing tissues: ornithine decarboxylase activity in regenerating rat liver, chick embryo, and various tumors. *Proc. Natl Acad. Sci. USA* **60**, 1420-1427.
20. Poulin, R., Pelletier, G. & Pegg, A.E. (1995). Induction of apoptosis by excessive polyamine accumulation in ornithine decarboxylase-overproducing L1210 cells. *Biochem. J.* **311**, 723-727.
21. Pegg, A.E. (1988). Polyamine metabolism and its importance in neoplastic growth and as a target for chemotherapy. *Cancer Res.* **48**, 759-774.
22. Auvinen, M., Paasinen, A., Andersson, L.C. & Holttä, E. (1992). Ornithine decarboxylase activity is critical for cell transformation. *Nature* **360**, 355-358.
23. Pegg, A.E., Shantz, L.M. & Coleman, C.S. (1995). Ornithine decarboxylase as a target for chemoprevention. *J. Cell Biochem. Suppl.* **22**, 132-138.
24. Bacchi, C.J., *et al.*, & Clarkson, A.B. Jr. (1994). Combination chemotherapy of drug-resistant *Trypanosoma brucei rhodesiense* infections in mice using DL- α -difluoromethylornithine and standard trypanocides. *Antimicrob. Agents Chemother.* **38**, 563-569.
25. Meyskens, F.L. Jr. & Gerner, E.W. (1995). Development of difluoromethylornithine as a chemoprevention agent for the management of colon cancer. *J. Cell Biochem. Suppl.* **22**, 126-131.
26. Mitchell, M.F., *et al.*, & Nishioka, K. (1998). Phase I dose de-escalation trial of α -difluoromethylornithine in patients with grade 3 cervical intraepithelial neoplasia. *Clin. Cancer Res.* **4**, 303-310.
27. Sandmeier, E., Hale, T.I. & Christen, P. (1994). Multiple evolutionary origin of pyridoxal-5'-phosphate-dependent amino acid decarboxylases. *Eur. J. Biochem.* **221**, 997-1002.
28. Momany, C., Ghosh, R. & Hackert, M.L. (1995). Structural motifs for pyridoxal-5'-phosphate binding in decarboxylases: an analysis based on the crystal structure of the *Lactobacillus 30a* ornithine decarboxylase. *Prot. Sci.* **4**, 849-854.
29. Grishin, N.V., Phillips, M.A. & Goldsmith, E.J. (1995). Modeling of the spatial structure of eukaryotic ornithine decarboxylase. *Prot. Sci.* **4**, 1291-1304.
30. Abrahamsen, M.S., Li, R.S., Dietrich-Goetz, W. & Morris, D.R. (1992). Multiple elements responsible for transcriptional regulation of the ornithine decarboxylase gene by protein kinase A. *J. Biol. Chem.* **267**, 18866-18873.
31. Reddy, S.G., *et al.*, & Haddox, M.K. (1996). Multisite phosphorylation of ornithine decarboxylase in transformed macrophages results in increased intracellular enzyme stability and catalytic efficiency. *J. Biol. Chem.* **271**, 24945-24953.
32. Rosenberg-Hasson, Y., Strumpf, D. & Kahana, C. (1991). Mouse ornithine decarboxylase is phosphorylated by casein kinase-II at a predominant single location (serine 303). *Eur. J. Biochem.* **197**, 419-424.
33. Hayashi, S., Murakami, Y. & Matsufuji, S. (1996). Ornithine decarboxylase antizyme: a novel type of regulatory protein. *Trends Biochem. Sci.* **21**, 27-30.
34. Heller, J.S., Fong, W.F. & Canellakis E.S. (1976). Induction of a protein inhibitor to ornithine decarboxylase by the end product of its reaction. *Proc. Natl Acad. Sci. USA* **73**, 1858-1862.
35. Mitchell, J.L. & Chen, H.J. (1990). Conformational changes in ornithine decarboxylase enable recognition by antizyme. *Biochim. Biophys. Acta* **1037**, 115-121.
36. Murakami, Y., *et al.*, & Ichihara, A. (1992). Ornithine decarboxylase is degraded by the 26S proteasome without ubiquitination. *Nature* **360**, 597-599.
37. Murakami, Y., Ichiba, T., Matsufuji, S. & Hayashi, S. (1996). Cloning of antizyme inhibitor, a highly homologous protein to ornithine decarboxylase. *J. Biol. Chem.* **271**, 3340-3342.
38. Fujita, K., Murakami, Y. & Hayashi, S. (1982). A macromolecular inhibitor of the antizyme to ornithine decarboxylase. *Biochem. J.* **204**, 647-652.
39. Kern, A., *et al.*, & Hackert, M.L. (1996). Crystallization of a mammalian ornithine decarboxylase. *Proteins* **24**, 266-268.
40. Ghoda, L., van Daalen Wetters, T., Macrae, M., Ascherman, D. & Coffino, P. (1989). Prevention of rapid intracellular degradation of ODC by a carboxyl-terminal truncation. *Science* **243**, 1493-1495.
41. Banner, D.W., *et al.*, & Waley, S.G. (1975). Structure of chicken muscle triose phosphate isomerase determined crystallographically at 2.5 Å resolution using amino acid sequence data. *Nature* **255**, 609-614.
42. Osterman, A.L., *et al.*, & Phillips, M.A. (1995). Domain organization and a protease-sensitive loop in eukaryotic ornithine decarboxylase. *Biochemistry* **34**, 13431-13436.
43. Coleman, C.S., Stanley, B.A., Viswanath, R. & Pegg, A.E. (1994). Rapid exchange of subunits of mammalian ornithine decarboxylase. *J. Biol. Chem.* **269**, 3155-3158.
44. Tobias, K.E., Mamroud-Kidron, E. & Kahana, C. (1993). Gly387 of murine ornithine decarboxylase is essential for the formation of stable homodimers. *Eur. J. Biochem.* **218**, 245-250.
45. Tobias, K.E. & Kahana, C. (1993). Intersubunit location of the active site of mammalian ornithine decarboxylase as determined by hybridization of site-directed mutants. *Biochemistry* **32**, 5842-5847.
46. Osterman, A.L., Grishin, N.V., Kinch, L.N. & Phillips, M.A. (1994). Formation of functional cross-species heterodimers of ornithine decarboxylase. *Biochemistry* **33**, 13662-13667.
47. Jones, S. & Thornton, J.M. (1996). Principles of protein-protein interactions. *Proc. Natl Acad. Sci. USA* **93**, 13-20.
48. Li, X. & Coffino, P. (1992). Regulated degradation of ornithine decarboxylase requires interaction with the polyamine-inducible protein antizyme. *Mol. Cell Biol.* **12**, 3556-3562.
49. Li, X. & Coffino, P. (1993). Degradation of ornithine decarboxylase: exposure of the C-terminal target by a polyamine-inducible inhibitory protein. *Mol. Cell Biol.* **13**, 2377-2383.
50. Tsirka, S. & Coffino, P. (1992). Dominant negative mutants of ornithine decarboxylase. *J. Biol. Chem.* **267**, 23057-23062.
51. Osterman, A.L., Brooks, H.B., Rizo, J. & Phillips, M.A. (1997). Role of Arg-277 in the binding of pyridoxal-5'-phosphate to *Trypanosoma brucei* ornithine decarboxylase. *Biochemistry* **36**, 4558-4567.
52. Osterman, A.L., Kinch, L.N., Grishin, N.V. & Phillips, M.A. (1995). Acidic residues important for substrate binding and cofactor reactivity in eukaryotic ornithine decarboxylase identified by alanine scanning mutagenesis. *J. Biol. Chem.* **270**, 11797-11802.
53. Yano, T., Mizuno, T. & Kagamiyama, H. (1993). A hydrogen-bonding network modulating enzyme function: asparagine-194 and tyrosine-225 of *Escherichia coli* aspartate aminotransferase. *Biochemistry* **32**, 1810-1815.
54. Brooks, H.B. & Phillips, M.A. (1997). Characterization of the reaction mechanism for *Trypanosoma brucei* ornithine decarboxylase by multiwavelength stopped-flow spectroscopy. *Biochemistry* **36**, 15147-15155.
55. Stamper, C.G.F., Morollo, A.A. & Ringe, D. (1998). Reaction of alanine racemase with 1-aminoethylphosphonic acid forms a stable external aldimine. *Biochemistry* **37**, 10438-10445.
56. Kirsch, J.F., Eichele, G., Ford, G.C., Vincent, M.G. & Jansonius, J.N. (1984). Mechanism of action of aspartate aminotransferase proposed on the basis of its spatial structure. *J. Mol. Biol.* **174**, 497-525.
57. Tobler H.P., Gehring, H. & Christen, P. (1987). Stereospecific labilization of the C-4' pro-S hydrogen of pyridoxamine 5'-phosphate in aspartate aminotransferase. *J. Biol. Chem.* **262**, 8985-8989.
58. Metzler, C.M., *et al.*, & Arnone A. (1988). Correlation of polarized absorption spectroscopic and X-ray diffraction studies of crystalline cytosolic aspartate aminotransferase of pig hearts. *J. Mol. Biol.* **203**, 197-220.
59. Julin, D.A. & Kirsch, J.F. (1989). Kinetic isotope effect studies on aspartate aminotransferase: evidence for a concerted 1,3 prototropic shift mechanism for the cytoplasmic isozyme and L-aspartate and dichotomy in mechanism. *Biochemistry* **28**, 3825-3833.
60. Toney, M.D. & Kirsch, J.F. (1993). Lysine 258 in aspartate aminotransferase: enforcer of the C_{irce} effect for amino acid substrates and general-base catalyst for the 1,3-prototropic shift. *Biochemistry* **32**, 1471-1479.
61. Malashkevich, V.N., Toney, M.D. & Jansonius, J.N. (1993). Crystal structures of true enzymatic reaction intermediates: aspartate and glutamate ketimines in aspartate aminotransferase. *Biochemistry* **32**, 13451-13462.

62. Hayashi, H., Mizuguchi, H. & Kagamiyama, H. (1998). The imine-pyridine torsion of the pyridoxal 5'-phosphate Schiff base of aspartate aminotransferase lowers its pKa in the unliganded enzyme and is crucial for the successive increase in the pKa during catalysis. *Biochemistry* **37**, 15076-15085.
63. Gani, D.A (1991). Structural and mechanistic comparison of pyridoxal-5'-phosphate dependent decarboxylase and transaminase enzymes. *Philos. Trans. R. Soc. Lond. B. Biol. Sci.* **332**, 131-139.
64. Coleman, C.S., Stanley, B.A. & Pegg, A.E. (1993). Effect of mutations at active site residues on the activity of ornithine decarboxylase and its inhibition by active site-directed irreversible inhibitors. *J. Biol. Chem.* **268**, 24572-24579.
65. Asada, Y., Tanizawa, K., Sawada, S., Suzuki, T., Misono, H. & Soda, K. (1981). Stereochemistry of meso- α,ϵ -diaminopimelate decarboxylase reaction: the first evidence for pyridoxal-5'-phosphate dependent decarboxylation with inversion of configuration. *Biochemistry* **20**, 6881-6886.
66. Asada, Y., Tanizawa, K., Nakamura, K., Moriguchi, M. & Soda, K. (1984). Stereochemistry of ornithine decarboxylase reaction. *J. Biochem.* **95**, 277-282.
67. Lim, Y. H., Yoshimura, T., Kurokawa, Y., Esaki, N. & Soda, K. (1998). Nonstereospecific transamination catalyzed by pyridoxal phosphate-dependent amino acid racemases of broad substrate specificity. *J. Biol. Chem.* **273**, 4001-4005.
68. Coffino, P. (1998) Degradation of Ornithine Decarboxylase. In *Ubiquitin and the Biology of the Cell*. (Peters, J.-M., Harris, J.R. and Finley, D., eds), pp. 411-428, Plenum Publishing, London.
69. Thiel, D.J., *et al.*, & Eikenberry, E.F. (1995). Macromolecular crystallographic results obtained at CHESS using a detector incorporating a charge-coupled device. *Rev. Sci. Instrum.* **66**, 1477-1479.
70. Otwinowski, Z. & Minor W. (1997). Processing of X-ray diffraction data collected in oscillation mode. *Methods Enzymol.* **276**, 307-326.
71. Otwinowski, Z. (1991). Maximum likelihood refinement of heavy atom parameters. In *Isomorphous Replacement and Anomalous Scattering*, (Wolff, W., Evans, P.R. & Leslie, A.G.W., eds), pp. 80-85 Daresbury Laboratory, Daresbury, UK.
72. Perrakis, A., Sixma, T.K., Wilson, K.S. & Lamzin, V.S. (1997). *wARP*: Improvement and extension of crystallographic phases by weighted averaging of multiple-refined dummy atomic models. *Acta Crystallogr. D* **53**, 448-455.
73. Jones, T.A., Zou, J.Y., Cowan, S., & Kjeldgaard M. (1991). Improved methods for building protein models in electron density maps and the location of errors in these models. *Acta Crystallogr. A* **47**, 110-119.
74. Brünger, A.T. (1992). *X-PLOR Version 3.1. A System for X-ray Crystallography and NMR*. Yale University Press, New Haven, CT.
75. Murshudov, G.N., Vagin, A.A. & Dodson, E.J. (1997). Refinement of macromolecular structures by the maximum-likelihood method. *Acta Crystallogr. D* **53**, 240-255.
76. Laskowski, R.A., MacArthur, M.W., Moss, D.S. & Thornton, J.M. (1993). PROCHECK: a program to check the stereochemical quality of protein structures. *J. Appl. Crystallogr.* **26**, 283-291.
77. Hoof, R.W.W., Vriend, G., Sander, C. & Abola, E.E. (1996). Errors in protein structures. *Nature* **381**, 272.
78. Kleywegt, G.J. (1997). Validation of protein models from C α coordinates alone. *J. Mol. Biol.* **273**, 371-376.
79. Collaborative Computational Project, Number 4 (1994). The CCP4 suite: Programs for Protein Crystallography. *Acta Crystallogr. D* **50**, 760-763.
80. Kraulis, P.J. (1991). MOLSCRIPT: A program to produce both detailed and schematic plots of protein structures. *J. Appl. Crystallogr.* **24**, 946-950.
81. Merrit, E.A. & Murphy, M.E.P. (1994). Raster3D Version 2.0. A program for photorealistic molecular graphics. *Acta Crystallogr. D* **50**, 869-873.
82. Nicholls, A., Sharp, K. & Honig, B. (1991). Protein folding and association: insights from the interfacial and thermodynamic properties of hydrocarbons. *Proteins* **11**, 281-296.
83. Esnouf, R.M. (1997). An extensively modified version of MolScript that includes greatly enhanced coloring capabilities. *J. Mol. Graph. Model.* **15**, 112-113, 132-134.

Because *Structure with Folding & Design* operates a 'Continuous Publication System' for Research Papers, this paper has been published on the internet before being printed (accessed from <http://biomednet.com/cbiology/str>). For further information, see the explanation on the contents page.